Carbohydrate Research 390 (2014) 76–80

Contents lists available at ScienceDirect

Carbohydrate Research

journal homepage: www.elsevier.com/locate/carres

Note

Theoretical insight into the pyrolytic deformylation of levoglucosenone and isolevoglucosenone

Ariel M. Sarotti *

Instituto de Química de Rosario, Facultad de Ciencias Bioquímicas y Farmacéuticas, Universidad Nacional de Rosario—CONICET, Suipacha 531, S2002LRK Rosario, Argentina

ARTICLE INFO

Article history:
Received 19 February 2014
Received in revised form 12 March 2014
Accepted 14 March 2014
Available online 22 March 2014

Keywords:
Levoglucosenone
Isolevoglucosenone
Pyrolytic deformylation
3-Oxidopyrylium
DFT

ABSTRACT

A computational study was conducted to gain insight into the pyrolytic deformylations of levoglucosenone and isolevoglucosenone. Present B3LYP/6-31G* and CBS-QB3 calculations provide valuable evidence to rule out the formation of isolevoglucosenone during the pyrolytic degradation of cellulosic materials. This, along with the supplementary data herein presented and with other recent reports, suggest that levoglucosenone should not be formed directly from levoglucosan (as proposed in numerous reports), but rather from another intermediate, such as 1,4:3,6-dianhydro-α-D-glucopyranose.

1. Introduction

The use of biomass as raw material for the production of fuels and chemical products has emerged as one of the most important fields in research activity, motivated by the severe problems of energy shortage and environmental pollution.[1] It is therefore not surprising that enormous effort is currently undertaken worldwide to convert biomass into highly valuable organic chemicals. Within this context, carbohydrates are the major annually renewable biofeedstocks from which to develop valuable chemicals that can compete, or even replace, those derived from petroleum.[2]

The pyrolytic decomposition of cellulosic materials (rapid heating in the absence of oxygen), is one of the most promising approaches for renewable production of valuable chemicals and fuels.[2] Among the extensive variety of organic compounds that can be obtained in this way, levoglucosenone (1,6-anhydro-3,4-dideoxy-β-D-*glycero*-hex-3-enopyranos-2-ulose) represents a versatile member of the carbohydrate family.[3,4] Apart from its highly functionalized structure, this enantiomerically pure bicyclic enone has an 1,6-anhydro bridge locking the pyranose ring in the $^1C_4$ conformation and sterically hinders the β-face of the molecule, ensuring high levels of π-facial selectivity in a wide variety of reactions.[3,4] For that reason, levoglucosenone has been highlighted as a very useful starting material for the synthesis of a wide variety of natural and synthetic compounds,[3,4] as well as for the development of new tools of asymmetric synthesis.[4,5]

It is well known that the product distribution from cellulose pyrolysis is sharply linked with the experimental conditions.[3,6] For instance, while the pyrolysis of untreated cellulose affords levoglucosan (1,6-anhydro-β-D-glucopyranose, (**1**) in up to 60% yield, the acid-treated cellulose affords levoglucosenone (**2**) in much lower yields (up to 10–12%).[3] However, the mechanism of cellulose pyrolysis is far from being completely understood, though important progresses have been recently published.[7]

The generation of levoglucosenone, formally a double dehydration of levoglucosan, represents an example of a transformation whose mechanism has not been fully elucidated yet. For instance, the complete absence of the transposed enone isolevoglucosenone (**3**) in the pyrolysates represents an experimental observation important to unravel. The first attempt to rationalize levoglucosenone formation was made by Broido and co-workers, and is depicted in Scheme 1.[8]

The key transformation, that defines the regiochemistry of the reaction products, involves a 1,2-hydride shift of the cation resulting from the dehydration of the OH group at C-3 of **1**. The pseudo-symmetry of the molecule allows two plausible shifts, namely A and B. In path A, the H-2 shifts to install the carbonyl group at C-2, leading to the formation of **2**, whereas in path B the hydride shift now occurs with the H-4 atom resulting in the ultimate generation of **3**. To explain the perfect selectivity in the dehydration process, the authors suggested that cation A should be more stabilized than cation B because of the proximity with the

* Tel.: +54 03414370477.
E-mail address: sarotti@iquir-conicet.gov.ar

http://dx.doi.org/10.1016/j.carres.2014.03.017
0008-6215/

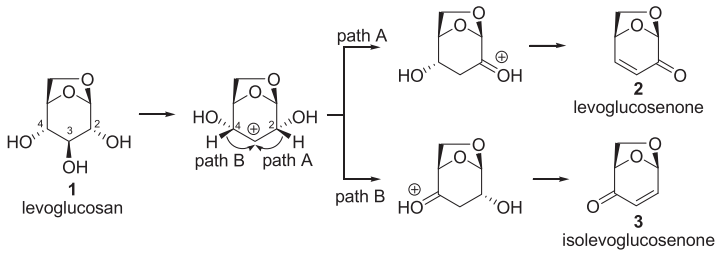

Scheme 1. Originally proposed mechanism of levoglucosenone formation.

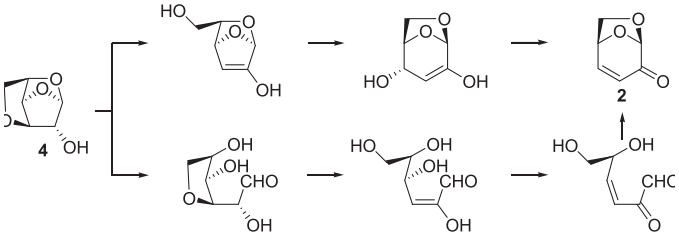

Scheme 2. Alternative proposal of 1,4:3,6-dianhydro-α-D-glucopyranose (**4**) as pyrolytic precursor or levoglucosenone.

1,6-anhydro oxygen atom.[8] However, according to calculations carried out in the present work at the high accuracy CBS-QB3 method, the regioselectivity of this dehydration step should be low. Very small energy differences between cations A and B ($\Delta\Delta G$ = 0.25 kcal/mol) and between the two 1,2-hydride shift transition structures connecting them with their precursor ($\Delta\Delta G^{\ddagger}$ = 0.21 kcal/mol) were computed.[9]

These results are in perfect agreement with a recent study of Assary and Curtiss, in which they provided further computational evidence of the dehydration process from **1** to **2** and **3**, in which the B3LYP/6-31G(2df,p) energy profiles computed for both pathways are similar in energy.[10]

A different approach was done by Shafizadeh et al. suggesting 1,4:3,6-dianhydro-α-D-glucopyranose (**4**), obtained from **1**, as a possible pyrolytic precursor of **2** (Scheme 2).[11] Interestingly, this proposal successfully explains the absence of **3** in the pyrolysates.

On the other hand, Furneaux et al. proved that **2** can undergo pyrolytic deformylation (via a [5+2] dipolar cycloreversion) to give formaldehyde (**5**) and 3-oxidopyrylium (**6**), a highly reactive species that can further dimerize or react with another molecule of **2** to afford adducts **7** and **8** in a 4:3 ratio.[12] The detection of these compounds in the pyrolysates evidenced not only the proposed degradation path, but also provided an explanation of the lower yield in which **2** is typically obtained with respect to **1**. Later, the same group found a similar chemical behavior for **3**: after heating, it suffers the loss of formaldehyde to afford **6**, that is further trapped by unreacted enone to yield the 1,3-dipolar adducts **9** and **10** in a 3:1 ratio (Scheme 3).[13] Interestingly, these adducts were not detected among the products from acid-catalyzed pyrolysis of cellulose, concluding that no evidence for the pyrolytic synthesis of **3** was found. However, it can be noted that these experimental observations (absence of **3**, **9,** and **10** in the pyrolysates) could be explained by assuming a faster thermolysis for **3** and a slower rate for its cycloaddition with **6**.

Understanding the pyrolysis process represents a key issue for the development of new technologies based on the generation of valuable chemicals from biomass. For that reason, a full computational study of the thermal deformylation of levoglucosenone and isolevoglucosenone was addressed.

First, the potential energy surface (PES) of the deformylation reactions was fully explored at the B3LYP/6-31G* level of theory, and the transition structures (TS) corresponding to each system were located (Fig. 1). As was found for other 1,3-dipolar cycloadditions, the concerted paths are favored.[14] In **TS-2**, the C5–C6 Wiberg bond index (WBI) is higher than that corresponding to the C1–O1 bonding (0.37 vs 0.26), while in the case of **TS-3** the bonding between C1–C6 is more developed than the C5–O1 bond formation (0.41 vs 0.24). The transition structure resulting from the deformylation of **3** is slightly more asynchronous than **TS-2**, both in terms of WBIs and bond lengths. IRC calculations yielded **TS-2** and **TS-3** as the only saddle points connecting reagents and products.

Both reactions are endergonic, mainly because of the relative instability of **5**. The calculated Gibbs free-energies of activation are also high, suggesting that they can only take place at high temperatures, in line with the experimental findings.[12,13] Interestingly, the barrier computed for **3** is 1.3 kcal/mol lower than that of **2**, indicating that the deformylation of the former should be faster as was hypothesized above. To validate this result, the high-accuracy composite method CBS-QB3 was next employed. The complete basis set (CBS) methods were developed by Petersson and co-workers to remove errors from the basis set truncation using asymptotic convergence of pair natural orbital expansions to extrapolate the estimated complete basis set limit.[15] The CBS-QB3, that starts on B3LYP/6-311G(d,p) geometries, has been found as a benchmark for predicting the activation barriers, reaction energetics and TS geometries of pericyclic reactions.[16] As depicted in Figure 1, B3LYP/6-31G* underestimates the $\Delta G^{\ddagger}$ and ΔG by about 5 kcal/mol and 8 kcal/mol, respectively, though the $\Delta\Delta G^{\ddagger}$ and $\Delta\Delta G$ values were nicely reproduced (1.2 kcal/mol and 0.2 kcal/mol, respectively).

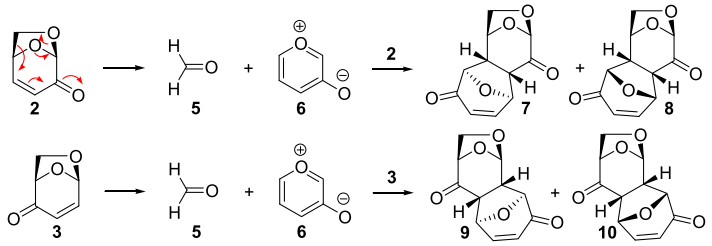

Scheme 3. Pyrolytic deformylation of **2** and **3**.

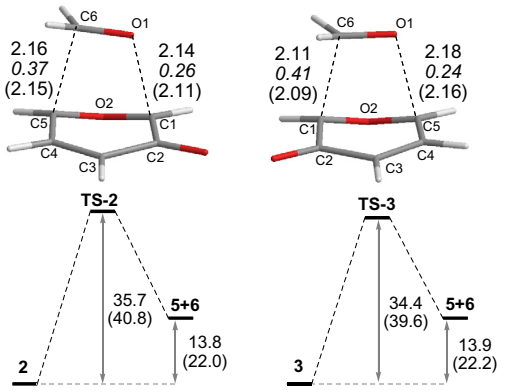

Figure 1. (a) B3LYP/6-31G* optimized geometries for the TSs of the deformylation reactions of levoglucosenone (**TS-2**) and isolevoglucosenone (**TS-3**), with selected distances in Å, WBIs (*in italics*) and CBS-QB3 distances (in parentheses). (b) Reaction profiles for both reactions, with Gibbs free energies (relative to the reactants) computed at the B3LYP/6-31G* and CBS-QB3 (in parentheses) levels.

Conceptual DFT analysis provided a powerful tool to understand the origins of these results.[17] Since **TS-2** and **TS-3** are regioisomeric transition structures, the analysis can be confined to searching the origins of the regioselectivity of the inverse reaction, that is, the 1,3-dipolar cycloaddition between **5** and **6**.

The static global properties, including the electronic chemical potential (μ), chemical hardness (η), global electrophilicity (ω), and global nucleophilicity (N) were computed at the B3LYP/6-31G* level of theory. The ω values of **6** and **5** are 2.46 and 1.45 eV, respectively, suggesting that the former is a more powerful electrophile.[18] In spite of that result, the electronic chemical potential of **5**, $\mu = -4.23$ eV, is lower than that of **6**, $\mu = -4.03$ eV, indicating that along the reaction coordinate the charge transfer (CT) will take place from **6** to **5**, in perfect agreement with the CT analysis performed at the TS (0.16 e for **TS-2** and 0.18 e for **TS-3**). This apparent contradiction can be easily understood considering the stronger nucleophilic character of **6** ($N = 3.43$ eV vs $N = 1.81$ eV). The electrophilic P^{+}_{k} and nucleophilic P^{-}_{k} Parr functions derived from the excess of spin density reached via a CT process accounts for the most favorable bond formation, that results from the coupling of C6, the most electrophilic center of **5** ($P^{+}_{k(C6)} = 0.74$ vs $P^{+}_{k(O1)} = 0.36$), and C1, the most nucleophilic center of **6** ($P^{-}_{k(C1)} = 0.40$ vs $P^{-}_{k(C5)} = 0.22$).[9] A better interaction in the transition structure connecting both centers should be expected, providing an explanation of the lower energy computed for **TS-3**.

Frontier molecular orbital (FMO) theory points in the same direction. The most important interaction is between the HOMO of **6** and the LUMO of **5** (energy gap = 4.5 eV), reinforcing the fact that the former is the nucleophilic counterpart in this reaction.

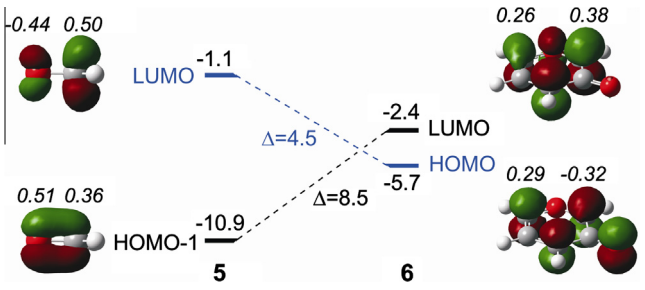

Figure 2. FMO interactions between **5** and **6**. Molecular orbital energies and energy gaps are given in eV. The 2pz coefficients are also shown (*in italics*).

Based on the coefficients of these FMOs (Fig. 2), the preferred interaction is expected to be between C1 of **6** and C6 of **5**, as found in **TS-3**.

The effect of a better overlap between interacting FMOs can be studied in detail from a distortion/interaction analysis. In this fragment approach, also known as the activation strain model, the activation energy, $\Delta E^{\ddagger}$, is decomposed as the sum of two main components: the distortion (or strain) energy, $\Delta E^{\ddagger}_{d}$, and the interaction energy, $\Delta E^{\ddagger}_{i}$. The $\Delta E^{\ddagger}_{d}$ is the energy required to distort the reactants from their initial geometries to their transition state geometries, while $\Delta E^{\ddagger}_{i}$ is the binding energy between the deformed fragments at the TS.[19]

Figure 3 shows the full activation-strain diagrams (the reaction profile $\Delta E(\zeta)$, along with its decomposition into the distortion energy (further decomposed in the distortion of both reagents) and the interaction energy between the deformed counterparts.

The $\Delta E^{\ddagger}_{d}$ accounts for the ~60% of the barrier heights, being the distortion of **6** the most relevant factor (~67% of the $\Delta E^{\ddagger}_{d}$). However, this energetic term shows little variation among the two paths under study (12.3 vs 13.0 kcal/mol). On the other hand, the strain of **5** is considerably larger (1.5 kcal/mol) in **TS-3** (5.6 vs 7.1 kcal/mol) because of the higher extent of pyramidalization. Overall, this transition structure is 2.2 kcal/mol more distorted than **TS-2**, indicating that the activation strain does not control the reactivity trends as was found for other pericyclic reactions.[14,20] Hence, the interaction energy must be responsible for the ease of deformylation of **3**. As depicted in Figure 3, while the ΔE_{i} is slightly positive (repulsive) for channel A at early stages of the reaction, the interaction energy computed for channel B is always negative (stabilizing). This trend remains along the path: in **TS-3** the binding energy of the deformed reagents is 3.7 kcal/mol stronger than in **TS-2** (−13.9 vs −10.2 kcal/mol). The better overlap of the FMO orbitals, and consequently the higher charge transfer, account for this observation.

Once the pyrolytic deformylation of levoglucosenone and its isomer isolevoglucosenone was fully understood, the computational study of the 1,3-dipolar cycloadditions between them and 3-oxidopyrylim (**6**) was next undertaken.

The electronic chemical potentials of **2** and **3**, $\mu = -4.14$ eV and −4.30 eV, respectively, are lower than that of **6**, $\mu = -4.03$ eV, indicating that the enones will receive charge transfer from the reactive 3-oxidopyrylium along the reaction coordinate, thus acting as the electrophilic counterparts. Small differences are computed for the electrophilic indexes of **2** and **3** (1.83 eV vs 1.93 eV, respectively), suggesting that the CT (and probably the $\Delta E^{\ddagger}_{i}$) would be similar at the corresponding TSs.[21] Analysis of the electrophilic Parr functions led to the expected result that the conjugated β carbons of the enones (C4) are the most electrophilic atoms in each system, and should interact preferentially with the most nucleophilic atom of the dipole (C1).

These results were further validated after a complete exploration of the PES corresponding to both reactions. Although up to eight isomeric products can be expected in each case, only the transition structures resulting from the attack of the dipole on the α face of the dipolarophiles were considered because it is well known that the β face of them is efficiently hindered by the 1,6-anhydro bridge.[3–5] Thus, four reaction channels for each system were computed, depending on the approach and orientation of the dipole toward dipolarophiles, namely *endo* (N)/*exo* (X), and *anti* (A)/*syn* (S). All TSs corresponding to each channel were located as the only saddle points connecting reagents and products after IRC calculations, and are shown in Figure 4.

The *anti* relationship was found to be considerably more stable (2.5–4.6 kcal/mol) than the *syn* approach, in line with the conceptual DFT analysis discussed above. In both cases, the *exo* approach is preferred over the *endo* orientation by 0.6–2.2 kcal/mol. The

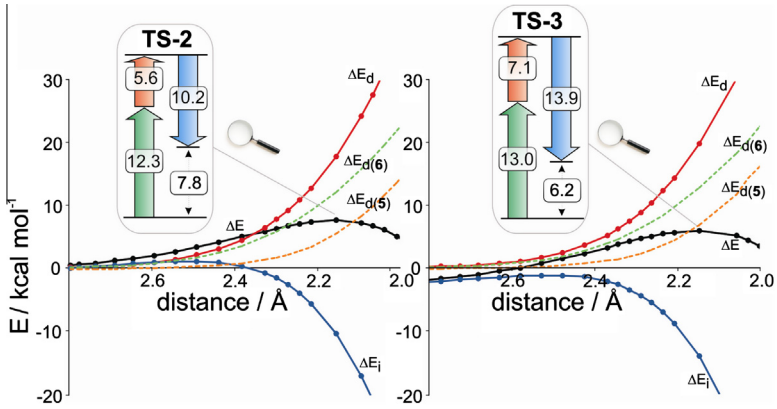

Figure 3. B3LYP/6-31G* activation-strain analysis of the 1,3-dipolar cycloaddition reaction between **5** and **6** along the reaction coordinate projected onto the average forming C–C and C–O distances.

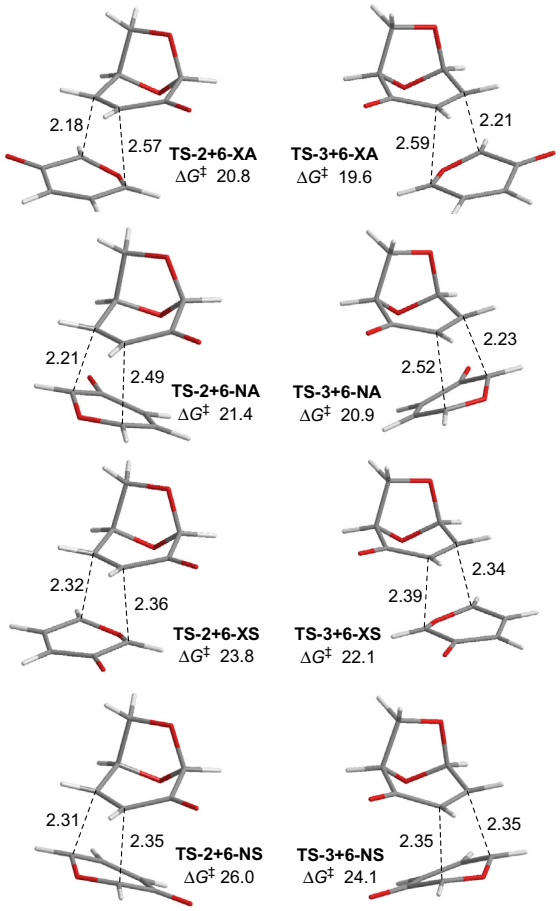

Figure 4. B3LYP/6-31G* optimized geometries for the TSs of the 1,3-dipolar cycloaddition reactions of enones **2**–**3** with 3-oxidopyrylium (**6**). Selected distances (in A) and Gibbs free energies of activation (in kcal/mol) are also given.

computed Gibbs free energy activation barriers for the reactions of **2**+**5** and **3**+**5** predict a XA/NA ratio of 63:37 and 75:25 at 600K, respectively, in excellent agreement with the product distribution of 57:43 and 75:25 experimentally found, respectively.[12,13]

Interestingly, despite the pseudo-enantiomeric relationship between both systems, the calculations show that isolevoglucosenone should be slightly more reactive than levoglucosenone toward 3-oxidopyrylium. The barrier heights computed for each channel of **3**+**6** are 0.5–1.9 kcal/mol lower in energy than the corresponding $\Delta E^{\ddagger}$ found for **2**+**6**. As expected from the ω values, the CT at the TSs are similar for each system (~0.1 e). Based on the computed bond forming distances (Fig. 4), there is a shift from late to early transition state when passing from **2**+**5** to **3**+**5**, as the activation barriers drop. As a consequence, **TSs-2**+**5** are more distorted than the corresponding **TSs-3**+**5**. For instance, **TS-2**+**5-XA** is 1.8 kcal/mol more distorted than **TS-3**+**5-XA**, being the $\Delta\Delta E^{\ddagger}_{i}$ only 0.6 kcal/mol.[9] As the binding energy of the deformed reactants shows little variation among each channel, the relative barrier heights are controlled by the strain energy.[14,20]

In summary, present B3LYP/6-31G* and CBS-QB3 calculations were carried out to understand the pyrolytic deformylation of levoglucosenone and isolevoglucosenone. The thermolysis of levoglucosenone requires larger activation barrier than that of isolevoglucosenone. This difference was interpreted on the basis of finely balanced geometric and electronic features at the TSs. In addition, the calculations suggest that isolevoglucosenone is slightly more reactive than levoglucosenone toward 3-oxidopyrylium. These results provide enough computational evidence to refute one of the original hypotheses formulated earlier. It would be difficult to explain the absence of **3** and its adducts with 3-oxidopyrylium (**9** and **10**) in the pyrolysis crudes without resorting to the idea that isolevoglucosenone does not form at all during the pyrolytic degradation of cellulosic materials. This, along with other recent reports, suggest that levoglucosenone should not be formed directly from levoglucosan, but rather from another intermediate, such as 1,4:3,6-dianhydro-α-D-glucopyranose.[11]

2. Computational methods

All calculations were performed using Gaussian 09.[22] Density functional theory (DFT) calculations were carried out with the B3LYP functional[23] with the standard 6-31G* basis set. High accuracy CBS calculations were carried out with the CBS-QB3 method.[15] Geometries for all structures were fully optimized and normal coordinate analyses were used to confirm the nature of the stationary points. All transition structures were confirmed to have only one imaginary frequency corresponding to the formation of the expected bonds. Intrinsic Reaction Coordinate (IRC) calculations were performed to determine the connections between stationary points. The electronic structures of TSs and ground states were analyzed in terms of the Wiberg bond indices (WBI) and the natural charges obtained from the Natural Bond Orbital (NBO) program as implemented in Gaussian 09.[24] Reported thermochemical properties include zero-point energies (ZPEs) without scaling and were calculated at 1 atm and 298.15 K.

Distortion energies were computed by performing a single point energy calculation using B3LYP/6-31G* on each of the separated, distorted fragments. The global electrophilicity index, ω, has been given by the following expression, $\omega = \mu^2/2\eta$, in terms of the electronic chemical potential μ and the chemical hardness η. Both quantities may be approached in terms of the one-electron energies of the frontier molecular orbitals HOMO and LUMO, εH and εL, as $\mu \sim (\varepsilon H + \varepsilon L)/2$ and $\eta \sim (\varepsilon L - \varepsilon H)$, respectively.[25] The nucleophilicity index, *N*, was computed as $N = E_{HOMO(diene)} - E_{HOMO(TCE)}$ (eV),[26] where TCE accounts for tetracyanoethylene. The local electrophilic indices, ω_k,[27] were computed according to the following expression: $\omega_k = \omega.P^+_k$, where P^+_k is the electrophilic Parr function of atom *k*,[28] that was computed using the Mulliken atomic spin density (ASD) computed by single-point UB3LYP/6-31G* level of the anion resulting from adding one electron to the optimized neutral B3LYP/6-31G* geometry.

Acknowledgements

This research was supported by ANPCyT, CONICET and UNR from Argentina.

Supplementary data

Supplementary data (full details of computational methods, additional computational results, coordinates and energies for all structures) associated with this article can be found, in the online version, at http://dx.doi.org/10.1016/j.carres.2014.03.017.

References

1. Klass, D. L. *Biomass for Renewable Energy, Fuels and Chemicals*; Academic Press: New York, USA, 1998.
2. (a) Lichtenthaler, F. W. *Acc. Chem. Res.* **2002**, *35*, 728–737; (b) Huber, G. W.; Iborra, S.; Corma, A. *Chem. Rev.* **2006**, *106*, 4044–4098; (c) Corma, A.; Iborra, S.; Velty, A. *Chem. Rev.* **2007**, *107*, 2411–2502.
3. (a)*Levoglucosenone and Levoglucosans: Chemistry and Applications*; Witczak, Z. J., Ed.; ATL Press: Mount Prospect, USA, 1994; (b)*Carbohydrate Synthons in Natural Products Chemistry. Synthesis, Functionalization, and Applications*; Witczak, Z. J., Tatsuta, K., Eds.ACS Symposium Series 841; American Chemical Society: Washington, DC, USA, 2003.
4. (a) Sarotti, A. M.; Zanardi, M. M.; Spanevello, R. A.; Suárez, A. G. *Curr. Org. Synth.* **2012**, *9*, 439–459; (b) Corne, V.; Botta, M. C.; Giordano, E. D. V.; Giri, G. F.; Llompart, D. F.; Biava, H. D.; Sarotti, A. M.; Mangione, M. I.; Mata, E. G.; Suárez, A. G.; Spanevello, R. A. *Pure Appl. Chem.* **2013**, *85*, 1683–1692.
5. For leading references, see: (a) Sarotti, A. M.; Spanevello, R. A.; Suárez, A. G.; Echeverría, G. A.; Piro, O. E. *Org. Lett.* **2012**, *14*, 2556–2559; (b) Sarotti, A. M.; Fernández, I.; Spanevello, R. A.; Sierra, M. A.; Suárez, A. G. *Org. Lett.* **2008**, *10*, 3389–3392; (c) Sarotti, A. M.; Spanevello, R. A.; Suárez, A. G. *Tetrahedron* **2009**, *65*, 3502–3508.
6. Sarotti, A. M.; Spanevello, R. A.; Suárez, A. G. *Green Chem.* **2007**, *9*, 1137–1140.
7. (a) Lin, Y. C.; Cho, J.; Tompsett, G. A.; Westmoreland, P. R.; Huber, G. W. *J. Phys. Chem. C* **2009**, *113*, 20097–20107; (b) Seshadri, V.; Westmoreland, P. R. *J. Phys. Chem. A* **2012**, *116*, 11997–12013; (c) Agarwal, V.; Dauenhauer, P. J.; Huber, G. W.; Auerbach, S. M. *J. Am. Chem. Soc.* **2012**, *134*, 14958–14972.
8. Halpern, Y.; Riffer, R.; Broido, A. *J. Org. Chem.* **1973**, *38*, 204–209.
9. For further details on this issue, see the Supplementary Data.
10. Assary, R. S.; Curtiss, L. A. *ChemCatChem* **2012**, *4*, 200–205.
11. Shafizadeh, F.; Furneaux, R. H.; Stevenson, T. T.; Cochran, T. G. *Carbohydr. Res.* **1978**, *61*, 519–528.
12. Furneaux, R. H.; Mason, J. M.; Miller, I. J. *J. Chem. Soc., Perkin Trans. 1* **1984**, 1923–1928.
13. Furneaux, R. H.; Gainsford, G. J. *Carbohydr. Res.* **1986**, *146*, 113–128.
14. Ess, D. H.; Houk, K. N. *J. Am. Chem. Soc.* **2008**, *130*, 10187–10198.
15. (a) Montgomery, J. A.; Frisch, M. J.; Ochterski, J. W.; Petersson, G. A. *J. Chem. Phys.* **2000**, *112*, 6532–6542; (b) Montgomery, J. A.; Frisch, M. J.; Ochterski, J. W.; Petersson, G. A. *J. Chem. Phys.* **1999**, *110*, 2822–2827; (c) Petersson, G. A.; Malick, D. K.; Wilson, W. G.; Ochterski, J. W.; Montgomery, J. A.; Frisch, M. J. *J. Chem. Phys.* **1998**, *109*, 10570–10579.
16. Guner, V.; Khuong, K. S.; Leach, A. G.; Lee, P. S.; Bartberger, M. D.; Houk, K. N. *J. Phys. Chem. A* **2003**, *107*, 11445–11459.
17. Geerlings, P.; De Proft, F.; Langenaeker, W. *Chem. Rev.* **2003**, *103*, 1793–1874.
18. Domingo, L. R.; Aurell, M. J.; Pérez, P.; Contreras, R. *Tetrahedron* **2002**, *58*, 4417–4423.
19. van Zeist, W.-J.; Bickelhaupt, F. M. *Org. Biomol. Chem.* **2010**, *8*, 3118–3127.
20. For leading references, see: (a) Lopez, S. A.; Houk, K. N. *J. Org. Chem.* **2013**, *78*, 1778–1783; (b) Fernández, I.; Bickelhaupt, F. M. *J. Comput. Chem.* **2012**, *33*, 509–516; (c) Fernández, I.; Cossío, F. P.; Bickelhaupt, F. M. *J. Org. Chem.* **2011**, *76*, 2310–2314; (d) Paton, R. S.; Kim, S.; Ross, A. G.; Danishefsky, S. J.; Houk, K. N. *Angew. Chem., Int. Ed.* **2011**, *50*, 10366–10368; (e) Fernández, I.; Bickelhaupt, F. M.; Cossío, F. P. *Chem. Eur. J.* **2009**, *15*, 13022–13032; (f) Hayden, A. E.; Houk, K. N. *J. Am. Chem. Soc.* **2009**, *131*, 4084–4089; (g) Schoenebeck, F.; Ess, D. H.; Jones, G. O.; Houk, K. N. *J. Am. Chem. Soc.* **2009**, *131*, 8121–8133.
21. (a) Sarotti, A. M. *Org. Biomol. Chem.* **2014**, *12*, 187–199; (b) Sarotti, A. M.; Spanevello, R. A.; Suárez, A. G. *Tetrahedron Lett.* **2011**, *52*, 4145–4148.
22. Frisch, M. J. et al *Gaussian 09, Revision B.01*; Gaussian, Inc.: Wallingford CT, 2009.
23. (a) Lee, C.; Yang, W.; Parr, R. G. *Phys. Rev. B* **1988**, *37*, 785–789; (b) Becke, A. D. *J. Chem. Phys.* **1993**, *98*, 1372–1377; (c) Becke, A. D. *J. Chem. Phys.* **1993**, *98*, 5648–5652.
24. NBO Version 3.1, Glendening, E. D.; Reed, A. E.; Carpenter, J. E.; Weinhold, F. For some original literature references, see: (a) Reed, A. E.; Weinstock, R. B.; Weinhold, F. *J. Chem. Phys.* **1985**, *83*, 735–746; (b) Reed, A. E.; Curtiss, L. A.; Weinhold, F. *Chem. Rev.* **1988**, *88*, 899–926.
25. (a) Parr, R. G.; Pearson, R. G. *J. Am. Chem. Soc.* **1983**, *105*, 7512–7516; (b) Parr, R. G.; Yang, W. *Density Functional Theory of Atoms and Molecules*; Oxford University Press: New York, 1989.
26. Domingo, L. R.; Chamorro, E.; Pérez, P. *J. Org. Chem.* **2008**, *73*, 4615–4624.
27. Domingo, L. R.; Aurell, M. J.; Pérez, P.; Contreras, R. *J. Phys. Chem. A* **2002**, *106*, 6871–6875.
28. Domingo, L. R.; Pérez, P.; Sáez, J. A. *RSC Adv.* **2013**, *3*, 1486–1494.